Supplementary material

Interactive visual exploration of 3D Mass Spectrometry Imaging Data using Hierarchical Stochastic Neighbor Embedding Reveals Spatio-Molecular Structures at Full Data Resolution

Walid M. Abdelmoula[1,2], Nicola Pezzotti[3], Thomas Hölt[3,4], Jouke Dijkstra[1], Anna Vilanova[3] , Liam A. McDonnell[5,6,#], Boudewijn P.F. Lelieveldt[1,3,#,*]

[1]*Division of Image Processing, Department of Radiology; Leiden University Medical Center, 2333 ZA Leiden, the Netherlands;* [2]*Department of Neurosurgery, Brigham and Women's Hospital, Harvard Medical School, Boston, MA 02115, USA;* [4]*Computational Biology Center;* [5]*Center for Proteomics and Metabolomics; Leiden University Medical Center, 2333 ZA Leiden, the Netherlands*
[3]*Computer Graphics and Visualization Group, Faculty of EEMCS, Delft University of Technology, 2628 CN Delft, The Netherlands*
[6]*Fondazione Pisana per la Scienza ONLUS, 56121 Pisa, Italy*

[#]***Contributed equally***

**** Corresponding author:***

Prof.dr.ir. Boudewijn Lelieveldt
B.P.F.Lelieveldt@lumc.nl
Phone: +31-(0)71 -52-63935
Division of Image Processing
Department of Radiology, 1-C2S
Leiden University Medical Center
P.O. Box 9600
2300 RC Leiden
The Netherlands

Table of Contents:

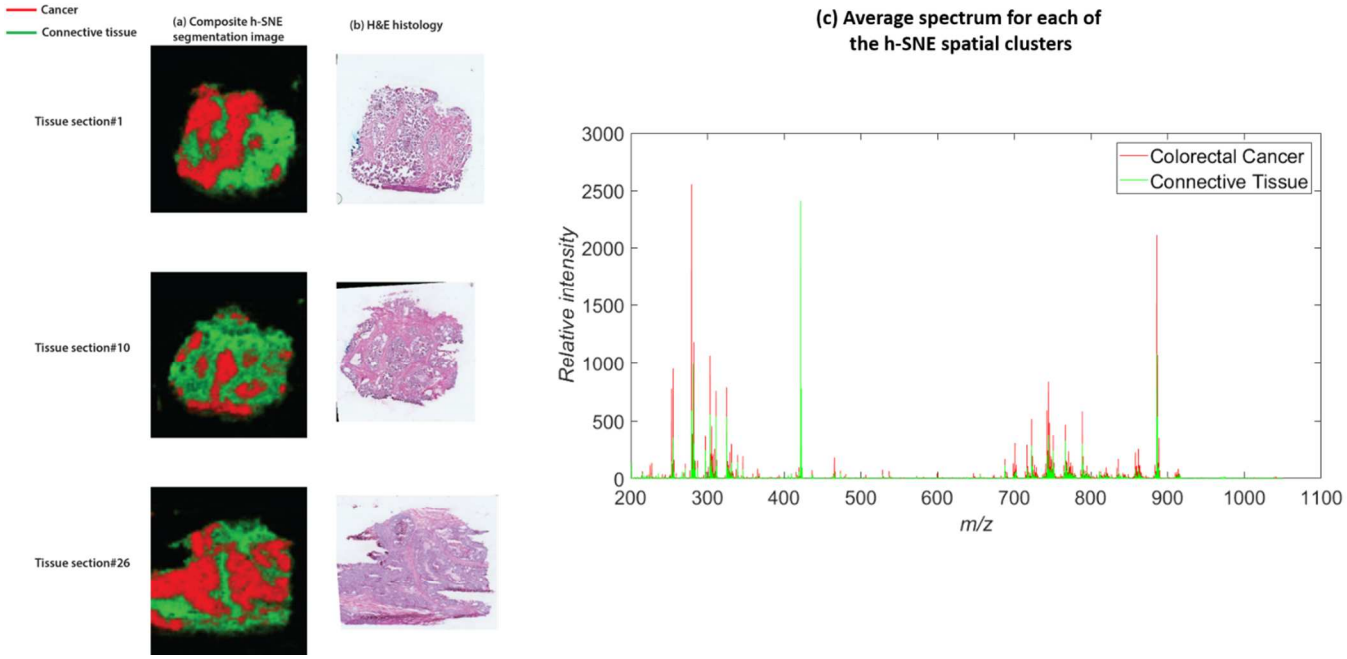

Figure S1. In concordance with histopathological examination of H&E images that confirms presence of two major tissue types (tumor and connective tissue), the spatial h-SNE segmentation maps of 3D MSI colorectal carcinoma data also demarcate perfectly these two tissue types (a-b). (C) Average spectrum distribution for each of these two h-SNE clusters; reflecting the intrinsic characteristics of their associated h-SNE landmarks.

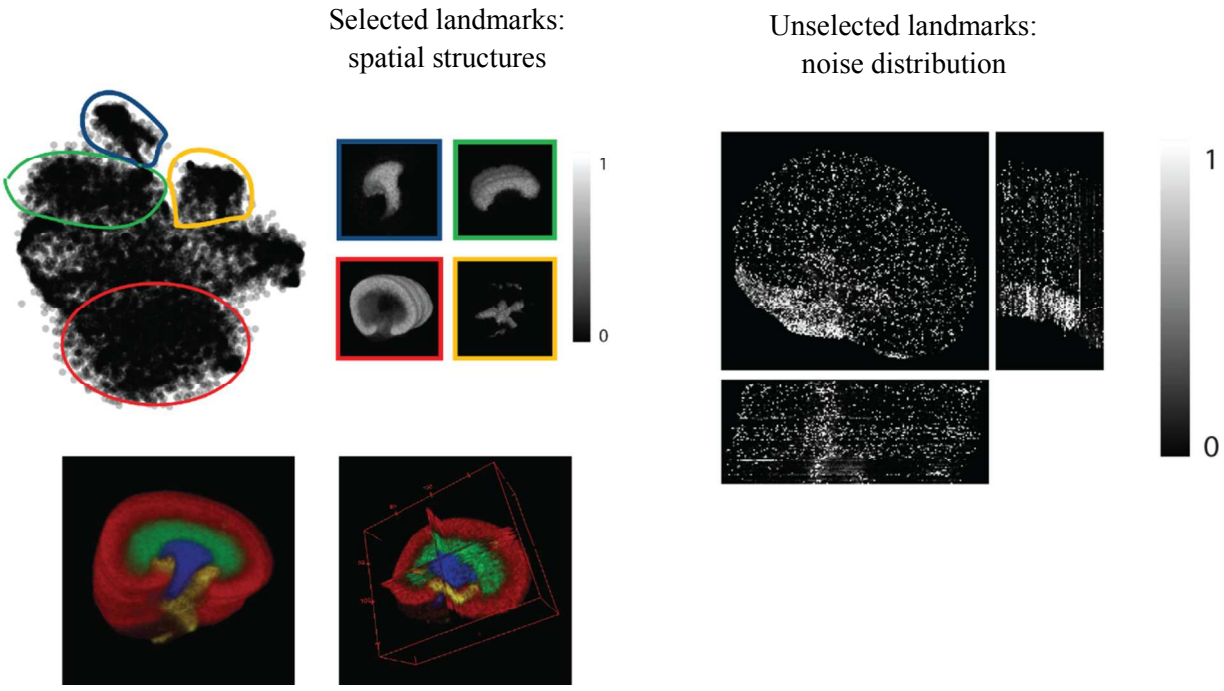

Figure S2. Analysis of 3D MALDI-MSI data of a mouse kidney using the HSNE. Selected landmarks in the HSNE embedding show informative spatial structures, whereas the landmarks not selected in this embedding represent noise-related structures.

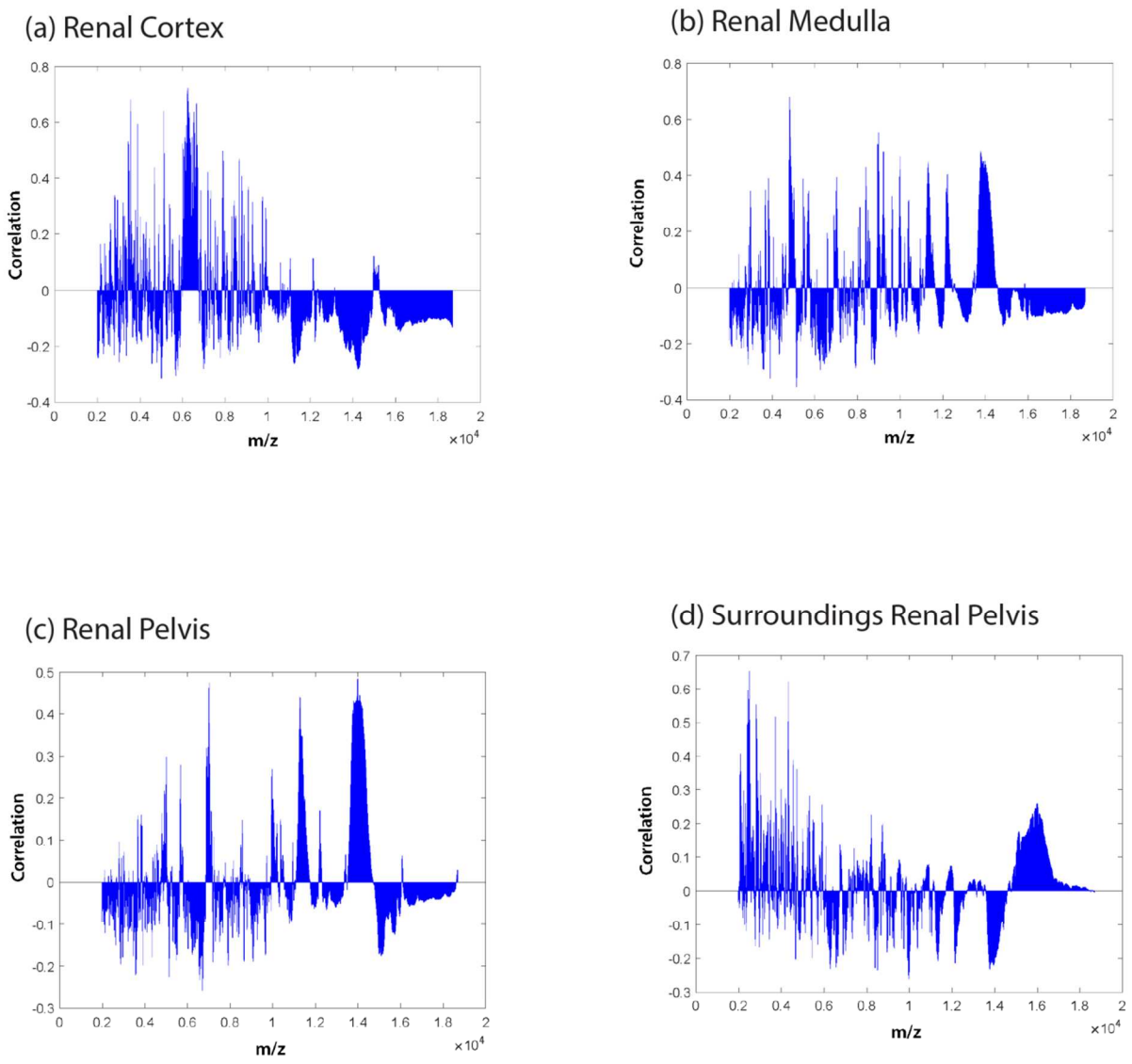

Figure S3. Spectral correlation distribution for each of the HSNE spatial segmentation maps of: a) renal cortex, b) renal medulla, c) renal pelvis, and d) surroundings of renal pelvis.

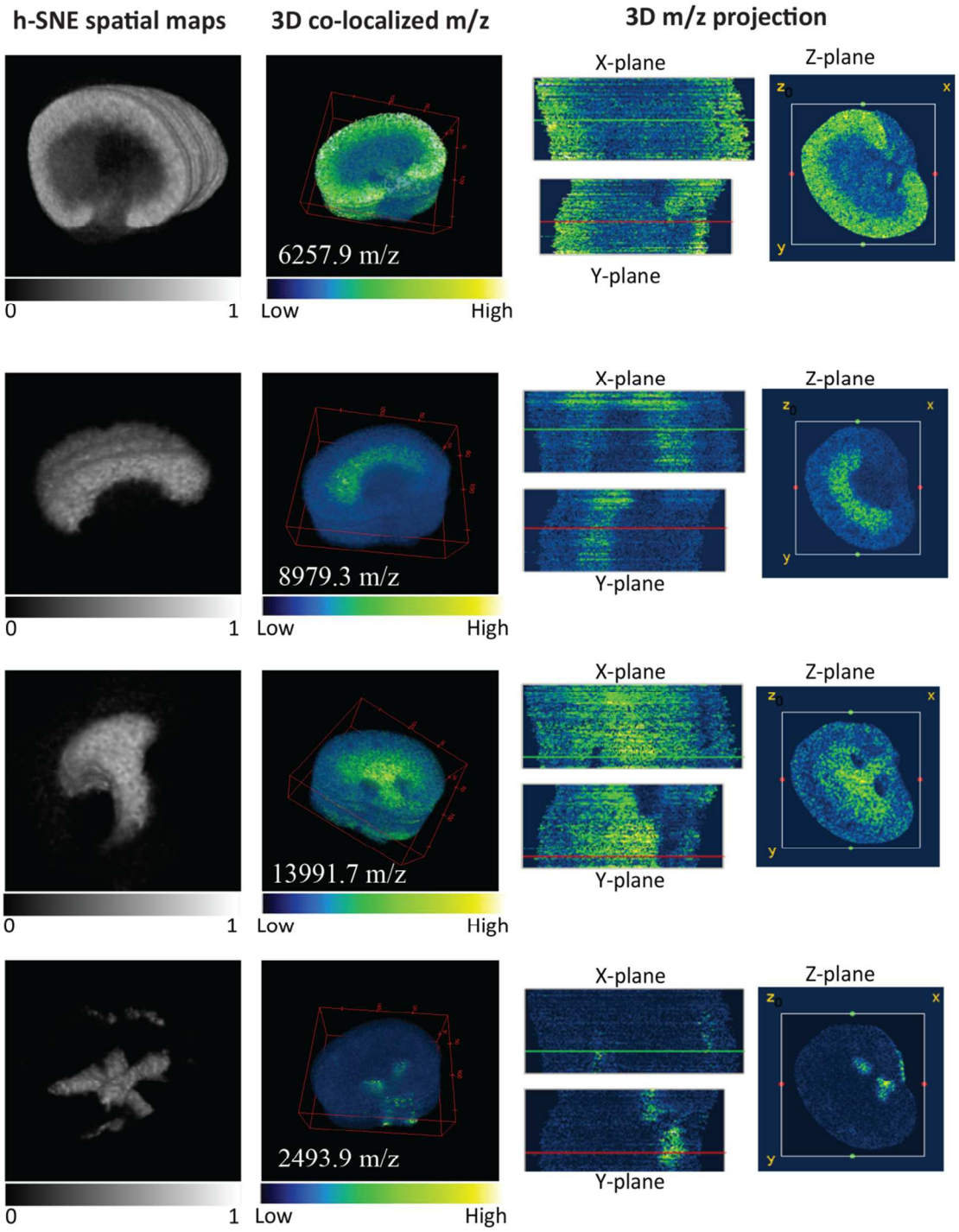

Figure S4. Visualization of the most co-localized 3D m/z features with respect to the associated HSNE spatial segmentation maps of the 3D MALDI-MSI mouse kidney dataset. The projection of the 3D co-localized m/z feature visualizes the expression across different X, Y, and Z planes.

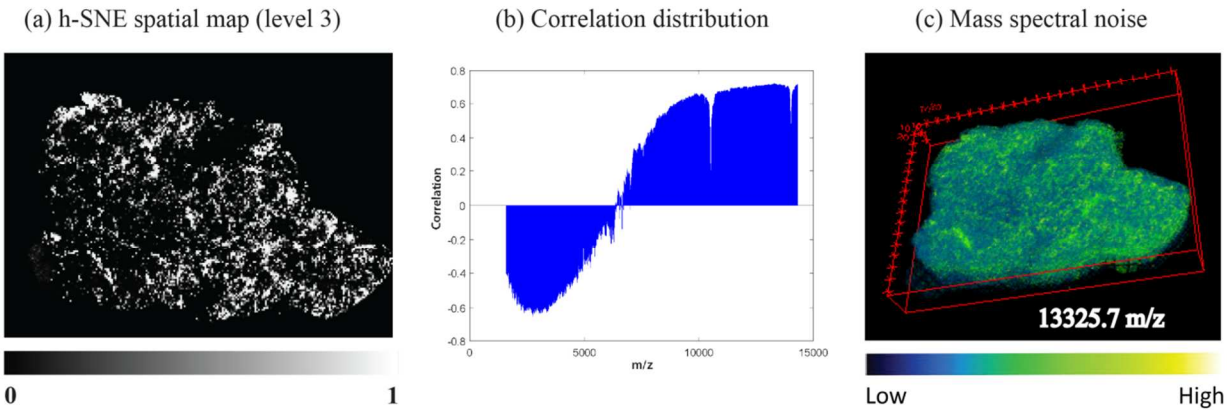

Figure S5. The HSNE spatial segmentation of one of the dominant foreground structures (structure1 shown in Figure 4a) identified by analyzing 3D MSI mouse pancreas data. Its spectral correlation distribution(b) revealed it is correlated with spatially mass spectral noise (c).

(a) Average mass spectra of two tissue sections

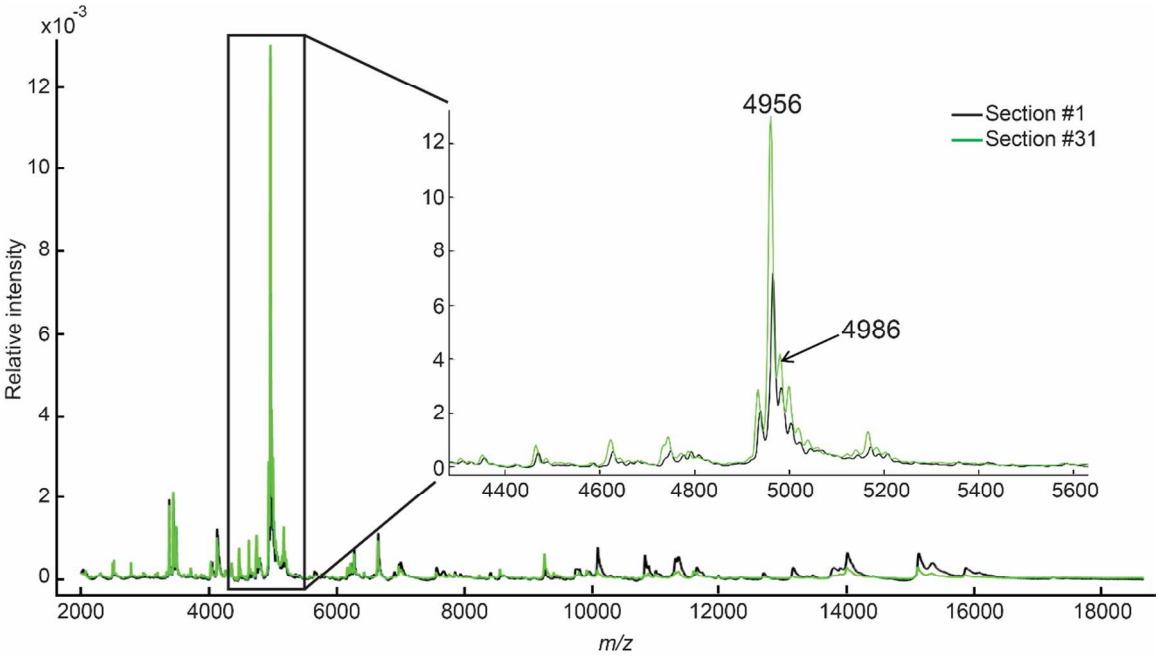

(b) Average distribution of two m/z features across the tissue sections

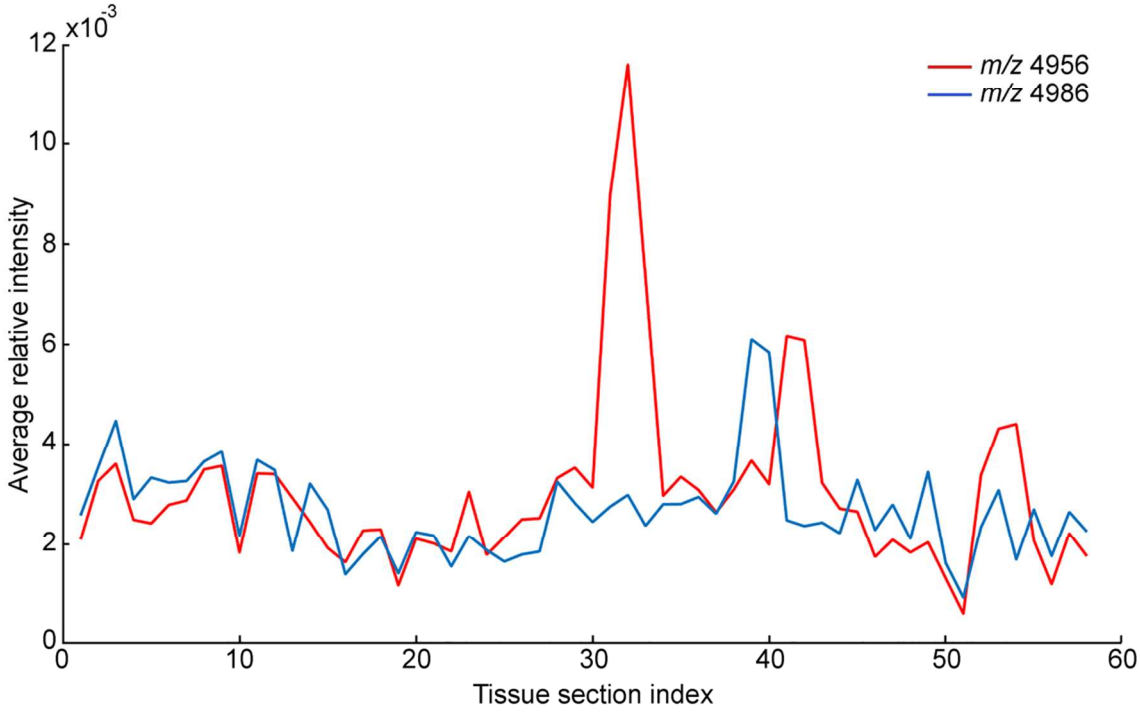

Figure S6. Three tissue sections (number 31, 32, and 33) from the 3D MALDI-MSI OSCC dataset suffer from batch effect at m/z 4956 (thymosin β4 signals). Average mass spectra distribution in a normal tissue section and a batch affected one (a), and (b) shows clearly localization of batch affected tissues in the 3D MSI dataset at m/z 4956.

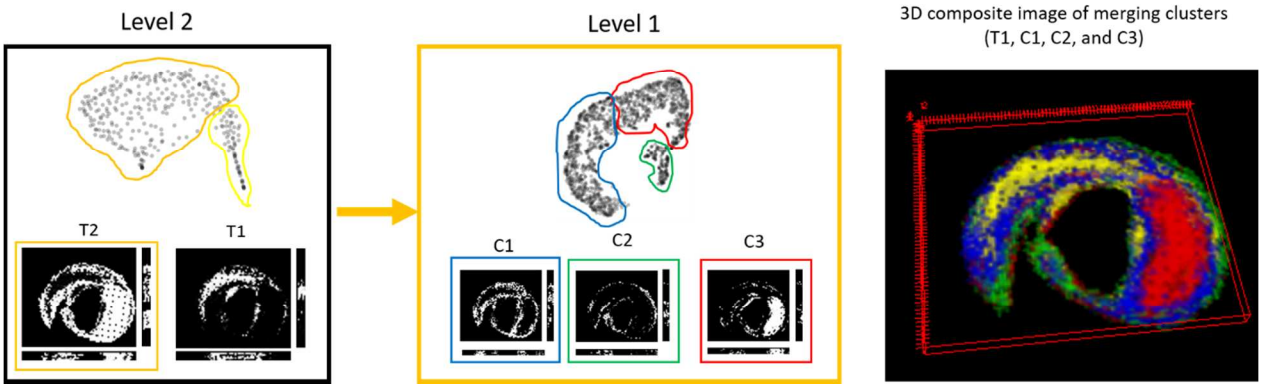

Figure S7. HSNE analysis of 3D-MALDI MSI dataset of Atherosclerotic plaque from human carotid shows distinct molecular regions, namely: 1) inner plaque (yellow and blue clusters), 2) middle plaque (red cluster), 3) outer plaque (green cluster).

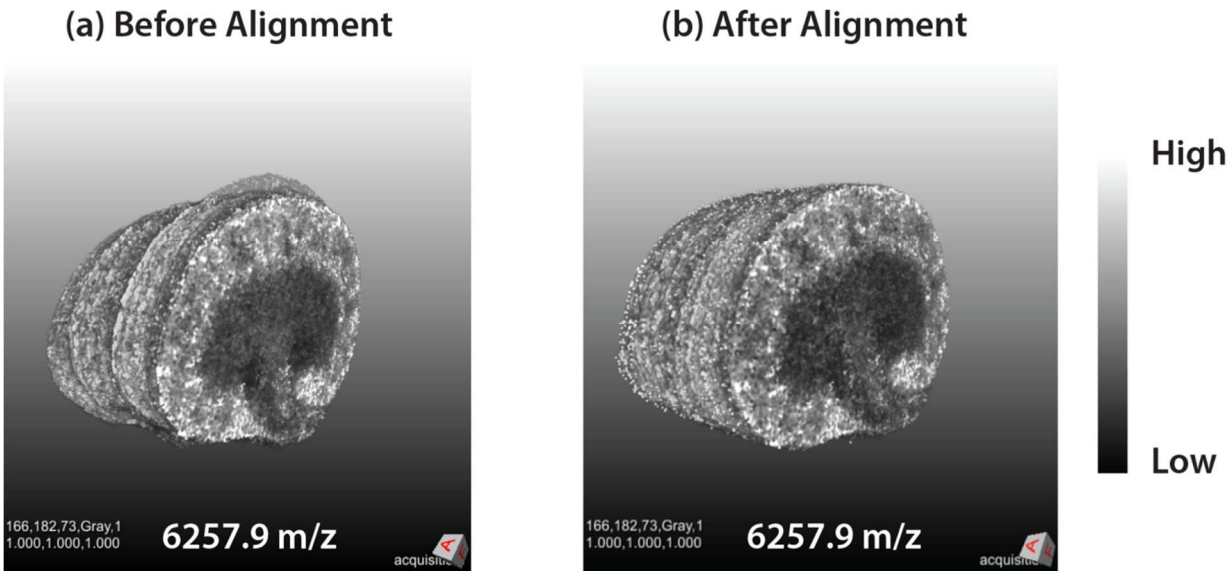

Figure S8. Automatic linear alignment using Euler transform (rotation and translation) improves visualization of the reconstructed 3D image of co-localized ion feature in the renal cortex of mouse kidney.